

DOI: 10.1070/QEL16049

X-ray optical system for imaging laser plumes with a spatial resolution of up to 70 nm

A.N. Nechai, A.E. Pestov, V.N. Polkovnikov, N.N. Salashchenko, M.N. Toropov, N.I. Chkhalo, N.N. Tsybin, A.V. Shcherbakov

Abstract. **We consider an X-ray optical system which permits obtaining laser plume images at a wavelength of 13.5 nm with a resolution of up to 70 nm. The X-ray optical system comprises an X-ray Schwarzschild objective made up of two aspherical multilayer mirrors, a scintillator (YAG:Ce ceramics), which converts X-rays to the visible radiation, and a visible-optical system, which images the scintillator surface onto a CCD camera. The spatial resolution of the system is limited by the resolution of the optical system (0.7 μm) and the magnification (10×) of the X-ray objective and is as high as 70 nm. The effect of Schwarzschild objective mirror shapes on the spatial resolution is analysed. The profile of concave mirror aspherisation is considered, which provides the attainment of the diffraction-limited quality of the objective. Data are given for the quantum efficiency of the system at a wavelength of 13.5 nm. We describe the experimental test bench intended for studying the developed X-ray optical system and outline the first experimental data which illustrate its efficiency. Owing to the natural division into the 'X-ray' and 'visible' parts, the optical system under discussion permits an easy change of the magnification and the field of view without realigning the X-ray optical elements. The wavelength may be varied in a range between 3 and 40 nm by changing the multilayer mirrors.**

Keywords: *laser-produced plasma, soft X-ray radiation, Schwarzschild objective, X-ray image, scintillator, aspherics, multilayer mirrors.*

1. Introduction

Laser-produced plasma enjoys wide use in modern research and technological devices like, for instance, compact short-wavelength radiation sources, particle sources, and thermonuclear reaction drivers [1–5]. Laser plasma develops quite rapidly in time and is the site of the simultaneous progress of a variety of complex physical processes. To adequately describe and monitor the plasma state calls for the means of obtaining spectral information about it with spatial and temporal resolution.

To study the spatial and temporal state of laser plasmas, use is made of pinhole [6] and streak cameras [7]. The former permit obtaining the spatial resolution of a fraction of a millimetre, while streak cameras possess temporal resolution at a level of nano- and picoseconds and even higher, as well as permit writing data arrays which reflect the development of a 2D image in time [8, 9]. Both of these devices may be combined with crystal- or multilayer-mirror-based spectrometers for obtaining spectral information along with the spatial one [6, 10]. To record soft X-ray (SXR) images, wide use is made of image-converter tubes [11] and backside-illuminated CCDs [12].

The main disadvantages of pinhole cameras, which stem from limitations on the hole diameter, are a low light-gathering power and an insufficiently high spatial resolution. This makes them poorly suited for the investigation of objects of characteristic size smaller than the incident radiation wavelength, which arise, for instance, in the interaction of laser radiation with matter [13, 14]. Studying these objects invites observation systems with a resolution of 100 nm or higher.

To improve the spatial resolution and light-gathering power, use can be made of X-ray optical schemes based on Fresnel zone plates or multilayer mirrors [12, 15]. When employed in the SXR range, Fresnel zone plates exhibit several drawbacks, which significantly limit their use in plasma research. In particular, owing to the small geometric aperture and a short focal distance, which is inversely proportional to the radiation wavelength, in the SXR range the distance between the laser plume under investigation and the zone plate should be equal to several millimetres, which leads to its prompt failure. Strong chromatic aberrations (the requisite degree of monochromatisation – the recorded wavelength-to-spectral width ratio – ranges into the hundreds) permit obtaining high-quality X-ray images only in narrow spectral lines. This is possible only when studying 'low-density' laser plasmas, for instance with the use of gas targets [16]. Broader spectral lines blur the image.

Normal-incidence multilayer mirrors, which possess a high light-gathering power and high (tens of percent) reflectivities at normal radiation incidence, provide an alternative to zone plates [17, 18]. In the majority of papers (see, for instance, Refs [15, 19]), spherical mirrors at near-normal incidence angles were employed for constructing images. Due to high mirror reflectivities in Bragg peaks, their radiation reflected at normal incidence exceeds the incoherently reflected background radiation by three–four orders of magnitude, which provides a high signal-to-noise ratio. Because of the absence of chromatic aberrations, the spectral line widths have no effect on the image quality. However, the spatial resolution of these systems is limited by the geometrical

A.N. Nechai, A.E. Pestov, V.N. Polkovnikov, N.N. Salashchenko, M.N. Toropov, N.I. Chkhalo, N.N. Tsybin, A.V. Shcherbakov Institute for the Physics of Microstructures, Russian Academy of Sciences, ul. Akademicheskaya 7, Afonino, 603087 Kstovskii district, Nizhnii Novgorod region, Russia; e-mail: chkhalo@ipm.sci-nnov.ru

Received 8 February 2016
Kvantovaya Elektronika **46** (4) 347–352 (2016)
Translated by E.N. Ragozin

Table 1. Calculated focal spot diameters in the objective's image plane accounting for 50% and 80% of radiation energy.

Energy in a spot (%)	Focal spot diameter/μm					
	Classical SO			SO with primary mirror aspherisation		
	$\lambda = 0$	$\lambda = 3$ nm	$\lambda = 13.5$ nm	$\lambda = 0$	$\lambda = 3$ nm	$\lambda = 13.5$ nm
50	1.94	1.98	1.98	0.004	0.016	0.70
80	2.59	2.50	2.88	0.005	0.27	1.20

aberrations of the mirrors, primarily by astigmatism and spherical aberration, and the difficulties associated with attaining large system magnification coefficients. Typical resolution may amount to a few micrometres.

The use of a Schwarzschild objective (SO), which is made up of two spherical mirrors, is an alternative approach. As shown in Ref. [20], for a correct selection of mirror radii and the separation of the elements of the optical setup it is possible to cancel axial aberrations up to the 5th order. The axial character of the optical system minimises astigmatism. Systems of this kind have been employed for SXR imaging for a rather long time [21–23]. However, owing to the presence of spherical aberrations the so-called classical SO does not provide a high spatial resolution even in the case of perfect spherical surfaces, as shown in Table 1.

Another problem in the development of SO-based high-resolution systems is due to the relatively small magnification of a SO (not more than 50) as well as with the real spatial resolution of detection systems. The characteristic pixel size of an X-ray backside-illuminated CCD camera is equal to ~10 μm and the resolution of an image-converter tube amounts to about 20 μm. When a detection system is combined with an objective of even diffraction-limited quality, the resultant resolution is nevertheless equal to the ratio of detector resolution and the SO magnification: 10 μm/50 = 0.2 μm for a CCD camera and 20 μm/50 = 0.4 μm for an image-converter tube. That is why in practice SOs are employed in X-ray microscopes for irradiating the objects under investigation with quasi-monochromatic SXR radiation and not as high-resolution projection objectives. In this case, the absorption image is recorded on a photographic film or a photoresist.

In this work we propose the use of SOs for studying laser plasmas with a high, better than 100 nm, spatial resolution. Two problems were solved for attaining the requisite resolution. First, to provide the diffraction-limited quality in the SXR range we developed an SO with a moderate amplification ($10^{\times}$), in which the surface of the concave mirror was made aspheric for correcting spherical aberrations and broadening the field of view. Second, to provide numerical image recording with a high spatial resolution we developed a 2D detector comprising a scintillator (YAG:Ce ceramics), which converts X-ray radiation to visible light, an optical system, which images the scintillator surface on the matrix of a CCD camera with a 20-fold magnification, and the optical CCD video camera itself.

Our experiments were carried out on the test bench described in Ref. [24], in which an X-ray tube was replaced with a laser-plasma radiation source [25].

2. Experimental facility

Figure 1 depicts the X-ray optical scheme of our experiment. The main elements of the facility are a laser-plasma source (LPS) (*1*), an SO (*3*), and a digital detector (DD) (*5*). The

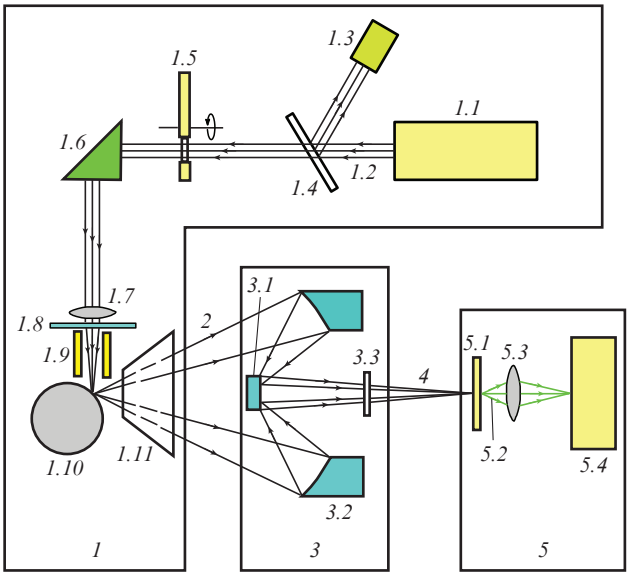

Figure 1. X-ray optical scheme of experiment: (*1*) LPS [(*1.1*) laser, (*1.2*) laser beam, (*1.3*) power meter, (*1.4*) beam splitter, (*1.5*) shutter, (*1.6*) prism, (*1.7*) short-focus lens, (*1.8*) protective quartz plate, (*1.9*) electromagnetic shield, (*1.10*) solid target, (*1.11*) electrostatic shield]; (*2*) polychromatic beam; (*3*) SO [(*3.1*) convex spherical mirror, (*3.2*) aspheric mirror, (*3.3*) cutoff filter]; (*4*) quasi-monochromatic beam; (*5*) digital detector [(*5.1*) scintillator, (*5.2*) visible radiation, (*5.3*) objective, (*5.4*) CCD camera].

polychromatic and quasi-monochromatic radiation beams at the output of the LPS and the SO are denoted by (*2*) and (*4*), respectively.

The LPS makes use of an Nd:YAG laser (*1.1*) with an output wavelength of 1.065 μm, a pulse duration of 9 ns, a pulse energy of 0.4 J, and a pulse repetition rate of 10 Hz. The laser power was monitored using a meter (*1.3*). Incident on the meter is the beam reflected from the beam splitter (*1.4*), which accounts for approximately 9% of initial beam power. A shutter (*1.5*) controls the passage and interception of a laser pulse. With a prism (*1.6*) the pulse is further directed to a focusing lens (*1.7*) with a focal length of 50 mm accommodated directly in a vacuum chamber and mounted on a bellows (not shown in the drawing). The latter serves to accurately focus the lens employing the recorded SXR signal. Located behind the lens is a replaceable thin quartz plate (*1.8*), which protects the lens from contamination by target erosion products. An additional protection stage, which minimises the contamination of the quartz plate, is a device with crossed electric (with a maximal voltage of 200 V) and magnetic (about 1000 Oe) fields. The laser radiation is focused on a target (*1.10*); the focal spot diameter is equal to about 100 μm. A part of the polychromatic radiation of the plasma (*2*) produced in the interaction of the

focused laser beam with the solid target propagates in the direction of the SO (*3*). Upon reflection from multilayer mirrors (*3.1*) and (*3.2*) and passage through a thin-film filter (*3.3*), which rejects the long-wavelength radiation (visible light, ultraviolet, and vacuum ultraviolet), monochromatic radiation (*4*) is incident on a scintillator (*5.1*) of the digital detector. To protect the objective's mirrors from contamination, use is made of electrostatic shield (*1.11*), which is a fan of metal plates with a voltage of 200 V applied across them.

The facility was evacuated using spiral backing, turbomolecular, and magnetic-discharge pumps, which provided a working vacuum at a level of 10^{-7} Torr. The shutter, the CCD camera, and the vacuum pumps were controlled with a computer, as was the collection of experimental data.

3. X-ray optical system

The X-ray optical system developed in the present work permits digital SXR imaging with a high spatial resolution. The system has two magnification stages. The first stage is an X-ray one, which magnifies an X-ray image to a degree such that, upon its conversion to the visible range, the image can be transformed by optical techniques and recorded with an inexpensive low-noise small-pixel CCD video camera without a sacrifice in spatial resolution. Let us consider the operation of the components of the system.

3.1. Projection aspheric SO

As noted above, in the execution of experiments to study laser plumes, X-ray optical elements should be located away from them to avoid contamination by erosion products and target damage. Practice suggests that a separation of several hundred millimetres is sufficient. However, a long separation of the primary objective mirror from the object under investigation does not permit obtaining a significant amplification with a SO. In view of the facility dimensions, a tenfold-magnifying classical SO with spherical mirrors was assumed as a basis [24]. The scaled objective schematic, the ray paths, and the basic dimensions in millimetres are shown in Fig. 2. The numerical aperture NA – the sine of the half angle subtended by the mirror at the source – is equal to 0.1. The radii of mirror curvature are R_{M1} = 428.50 mm and R_{M2} = 133.05 mm. The diffraction-limited resolution of this objective depends on the wavelength as $\delta x = 0.61\lambda/\mathrm{NA}$ or, considering the value of numerical aperture, $\delta x = 6.1\lambda$. For instance, for a wavelength of 10 nm the diffraction-limited spatial resolution amounts to about 60 nm.

In reality, owing to geometrical aberrations the classical SOs with spherical mirrors do not permit achieving the requisite resolution. To solve this problem, we calculated the aspheric profile of the M1 mirror surface shown in Fig. 3. Plotted on the abscissa are the distances of surface points from the mirror axis and plotted on the ordinate are the surface departures (etching depth) from the sphere. The ZEMAX code was used to calculate the optical system, including the aspherical profile. In the course of calculations, a point source of the spherical wave was placed in the object plane, where the laser plume was located, and the energy distribution was analysed in the focal spot in the image plane. We compared the results of simulations for the classical SO and an SO with an aspherical primary mirror. The calculated diameters of the focal spot containing 50% and 80% of energy are collected in Table 1. The focal spot diameters were calculated in the geometrical-optics approximation ($\lambda = 0$) and for wavelengths of 3 and 13.5 nm. In view of the system's magnification ($10^{\times}$), the focal spot diameter (the SO resolution) in the object plane is ten times smaller than the figures given in Table 1. For instance, the focal spot diameter for the aspherised SO at a wavelength of 13.5 nm containing 50% of the energy is equal to 700 nm, which corresponds to a resolution of 70 nm in the object plane. Therefore, when use is made of spherical mirrors, their aberrations do not permit obtaining a resolution of better than 200 nm, while the asphericisation of only one mirror makes it possible to obtain nanometre spatial resolution. To practically achieve a diffraction-limited image quality requires a relatively shallow (32 nm at most) asphericisation (Fig. 3).

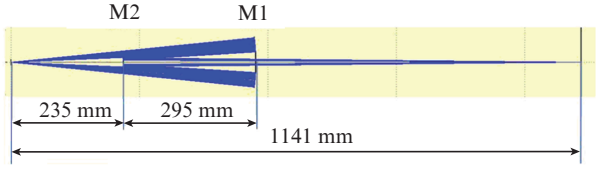

Figure 2. Scaled schematic of the SO and its basic dimensions (M1 is the concave spherical mirror, M2 is the convex spherical mirror).

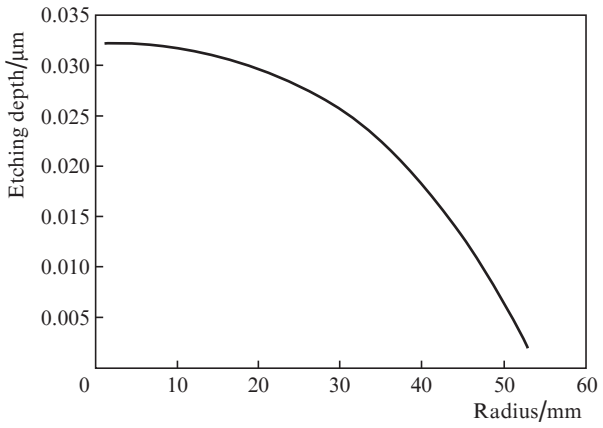

Figure 3. Calculated etching profile for spherical mirror M1.

In our experiment, the correction of local shape errors of mirror surfaces and the asphericisation of mirror M1 were made employing ion beam etching with the use of equipment and techniques described in Refs [18, 26–28]. Mo/Si multilayer mirrors optimised for a wavelength of 13.5 nm were deposited on the surfaces of objective mirrors by magnetron sputtering. The peak mirror reflectivities were equal to 66%, which corresponds to a two-mirror objective energy efficiency of 44% and, for NA = 0.1, permits collecting at the focal spot as much as 0.1% of the total power of the plasma plume radiation from the spectral band of the SO.

To eliminate parasitic illumination in the long-wavelength spectral range, use was made of free-standing thin-film filters with a transmission of 70% at a wavelength of 13.5 nm. The

techniques of depositing multilayer mirrors and fabricating free-standing filters as well as the methods of measuring their reflection and transmission coefficients are described in Refs [29, 30]. Figure 4 shows the photograph of the objective with the mirrors and filter in place. To change the operating wavelength, it would be sufficient to change the mirrors and the filter.

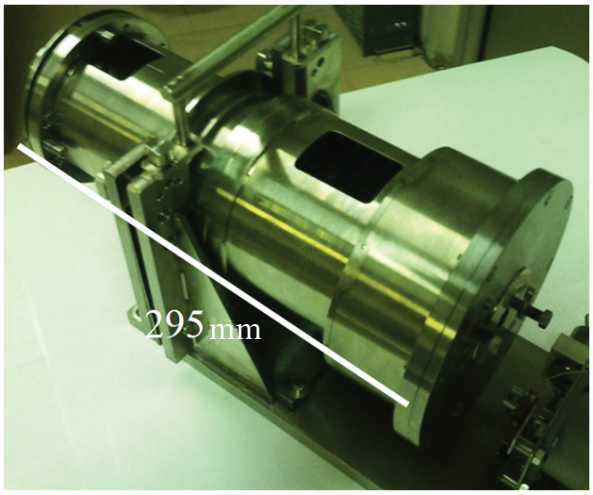

Figure 4. External appearance of the SO.

3.2. Two-coordinate digital detector

To realise the large magnification of the X-ray optical system and the digital image recording, we developed a special detector, which is schematised and photographed in Fig. 5. The main detector elements are a scintillator (*2*) and fast projection lens (*4*) with a field lens (*5*), which forms the image on a CCD camera (*6*).

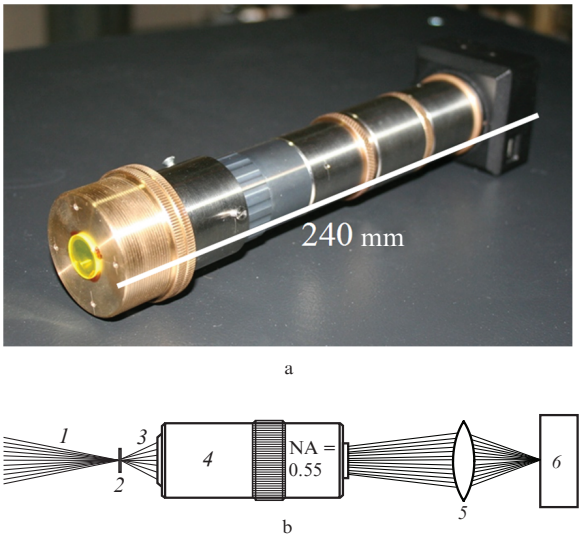

Figure 5. (a) Photograph and (b) schematic of a two-coordinate digital detector:
(*1*) incident X-rays; (*2*) scintillator; (*3*) reradiated visible light; (*4*) Mitutoyo Plan Apo optical objective; (*5*) imaging lens; (6) CCD camera.

The scintillator is a Ce : YAG ceramics, which converts the incident X-rays to visible radiation; the optical objective and the field lens relay the optical radiation to the CCD with 20-fold magnification. For an objective we selected a Mitutoyo Plan Apo lens. The choice was made because this objective is a part of a series of objectives with different numerical apertures; in this case, if use is made of a field lens with the recommended focal distance (200 mm), the objectives may be changed without varying the distances between the elements. To state it in different terms, the objectives may be changed, depending the requisite resolution and field of view, without changing the dimensions of the detector.

In the present design we selected the objective with NA = 0.55. In our experiment, the geometric aperture ratio of the detector, i.e. the fraction of the scintillator-reradiated light collected by the detector, was equal to 21.7%. Considering the geometric losses and the X-ray-to-visible radiation conversion coefficient equal to ~0.33 (an SXR radiation energy of 10.5 eV is expended to produce a visible light photon with an energy of 3.5 eV [31]), the energy efficiency of the entire detector amounted to 7.2%. This efficiency proved to be sufficient for recording the images of laser plumes produced using a relatively low-power laser-plasma source (see below). The detector made use of a BRM 1400HM-U CCD camera (ES EXPERTS, St. Petersburg).

4. Experimental results and their discussion

As follows from Table 1, the SO with an aspherised mirror provides a nanometre-scale spatial resolution, which is limited by SXR radiation diffraction. It is evident that the spatial resolution of the whole X-ray optical system is limited by the resolution of the optical objective, i.e. by the optical part of the system. To determine the spatial resolution of the optical part, we deposited an opaque metallic film on the X-ray-irradiated scintillator surface; strip-shaped openings with nominal widths of 0.7, 1.0, 1.5, and 2 μm were made in the film using electron-beam lithography. Next the detector was exposed to visible or SXR radiation in our facility, the resultant images were analysed, and the spatial detector resolution was estimated from the images. Figure 6 shows the recorded SXR image and the transverse lineout of the fringes of minimal width.

One can see from Fig. 7 that the results of measurements in the SXR and visible ranges agree nicely. In this case, the spatial resolution by the Rayleigh criterion is equal to 0.67 μm. Therefore, the limiting spatial resolution of the entire X-ray optical system is limited by the resolution of the optical objective, which is equal to 0.7 μm. In view of the SO's magnification ($10^{\times}$), this corresponds to a spatial resolution of ~70 nm.

Figure 7 depicts the image of a plasma plume recorded using the facility described in our work. The image was obtained for a 1-s exposure, i.e. the plume image averaged over 10 laser shots. The plume's inclination corresponds to the angle of incidence of laser radiation on the target. The overall size of the plume, which is elongated in the direction of laser radiation propagation, amounts to 100 × 150 μm (full width at half intensity).

In the present series of experiments we did not determine the overall (X-ray) resolution. To do this requires shifting the laser beam by several millimetres from the object plane and place a test object in it. At present we are looking for such an

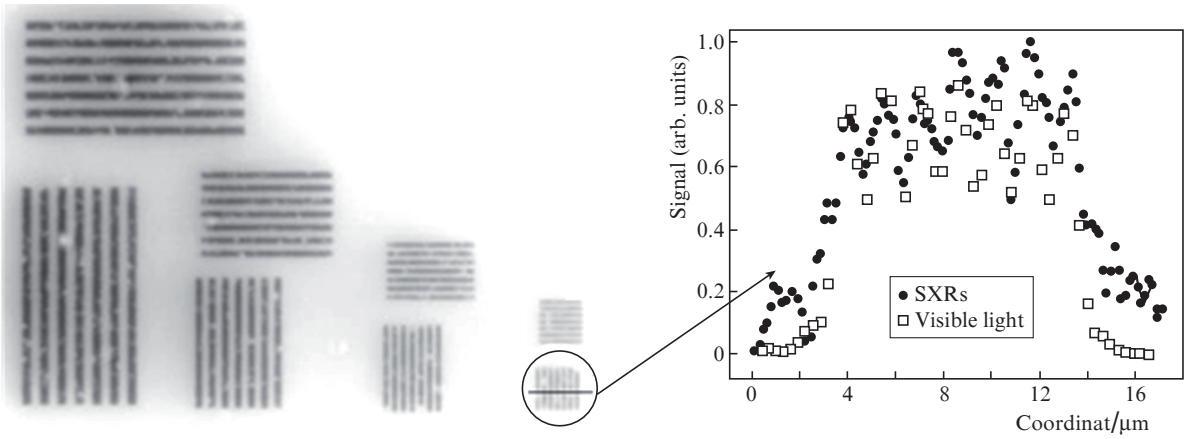

Figure 6. SXR image and lateral lineouts of the fringes of minimal width (encircled) obtained in the irradiation in the visible and SXR ranges.

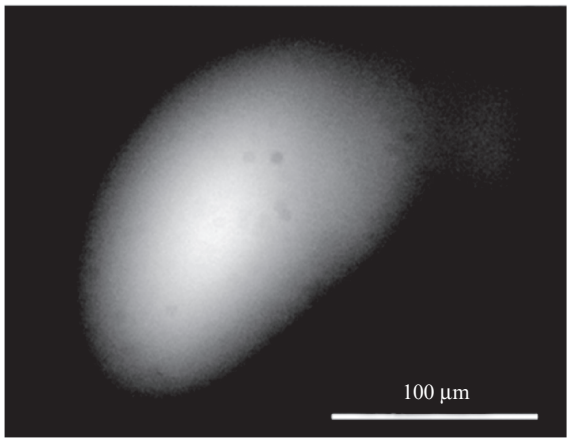

Figure 7. Laser plume image at a wavelength of 13.5 nm recorded using the X-ray optical system developed in our work.

object with characteristic dimensions of 70 nm that could survive in the course of experiments.

If need be, the resolution may be increased by a factor of 1.4–3 by using the Mitutoyo Plan Apo lens with NA = 0.75 and a SO with a 20-fold magnification. Our simulations bear out this possibility for the existing facility dimensions.

To summarise, we highlight the main results of our work. We proposed and made an X-ray optical system, which permits studying plasmas in the SXR range with a spatial resolution at a level of 70 nm. No direct resolution measurement was made in this range; however, the test data for objective aberrations, which did not exceed 1 nm, and the test data for the spatial resolution of the optical part of the system suggest strongly that the system does provide the indicated resolution. We also made a digital detector with a SXR-to-visible radiation conversion, which provides, according to out data, a record resolution in comparison with its analogues.

Acknowledgements. This work was supported by the Presidium of the Russian Academy of Science (Programme No. 21 'Extreme Laser Radiation: Physics and Fundamental Applications') and the Russian Foundation for Basic Research (Grant Nos 15-02-02139, 15-02-07660, 14-02-31436, and 14-02-00549).

References

1. Gillikson E.M., Underwood J.H., Batson P.C. et al. *J. X-ray Sci. Technol*., **3**, 283 (1992).
2. Young B.K., Wilson B.G., Price D.F., et al. *Phys. Rev*., **58**, 4929 (1998).
3. Banine V.Y., Koshelev K.N., Swinkels G.H. *J. Phys. D: Appl. Phys*., **44**, 253001 (2011).
4. Esarey E., Sprangle P., Krall J., et al. *IEEE Trans. Plasma Sci*., **24** (2), 252 (1996).
5. Hurricane O.A., Callahan D.A., Casey D.T., et al. *Nature*, **506**, 343 (2014).
6. Kantsyrev V.L., Bauer B.S., Shlyaptseva A.S., et al. *AIP Conf. Proc*., **409**, 499 (1997).
7. Rai V.N., Shukla M., Pant H.C., et al. *Sadhan*., **24** (6), 513 (1999).
8. Shiraga H., Nakasuji M., Heya M., et al. *Rev. Sci. Instrum*., **70**, 620 (1999).
9. Kodama R., Okada K., Kato Y. *Rev. Sci. Instrum*., **70**, 625 (1999).
10. Moos W., Zwicker A.P., Regan S.P., et al. *Rev. Sci. Instrum*., **61**, 2733 (1990).
11. Yamaguchi N., Katoh J., Cho T., et al. *Appl. Phys. Lett*., **60** (7), 821 (1992).
12. Wachulak P.W., Bartnik A., Fiedorowicz H., et al. *Opt. Express*, **19** (10), 9541 (2011).
13. Pirozhkov A.S., Kando M., Esirkepov T.Z., et al. *New J. Phys*., **16**, 093003 (2014).
14. Pirozhkov A.S., Kando M., Esirkepov T.Z., et al. *Phys. Rev. Lett*., **108**, 135004 (2012).
15. Seely J.F., Holland G.E., Giasson J.V. *Appl. Opt*., **32**, 31 (1993).
16. Rakowski R., Bartnik A., Fiedorowicz H., et al. *Appl. Phys. B*, **101**, 773 (2010).
17. Platonov Y., Rodriguez J., Kriese M., et al. *Proc. SPIE Int. Soc. Opt. Eng*., **8076**, 80760N (2011).
18. Barysheva M.M., Pestov A.E., Salashchenko N.N., et al. *Usp. Fiz. Nauk*, **182** (7), 727 (2012) [*Phys. Usp*., **55** (7), 681 (2012)].
19. Akhsakhalyan A.D., Kolachevsky N.N., Mitropolsky M.M., et al. *Phys. Scripta*, **48**, 516 (1993).
20. Hoover R.B., Shealy D.L., Gabardi D.R., et al. *Proc. SPIE Int. Soc. Opt. Eng*., **984**, 234 (1988).
21. Lovas I., Santy W., Spiller E., et al. *Proc. SPIE Int. Soc. Opt. Eng*., **316**, 90 (1981).
22. Tanaka K.A., Kado M., Kodama R., et al. *Proc. SPIE Int. Soc. Opt. Eng*., **1140**, 502 (1989).
23. Artyukov I.A., Asadchikov V.E., Vinogradov A.V., et al. *Kvantovaya Elektron*., **22** (9), 951 (1995) [*Quantum Electron*., **25** (9), 919 (1995)].

24. Aruev P.N., Barysheva M.M., Ber B.Ya., et al. *Kvantovaya Elektron*., **42** (10), 943 (2012) [*Quantum Electron*., **42** (10), 943 (2012)].
25. Zuev S.Yu., Pestov A.E., Salashchenko N.N., et al. *Izv. Ross. Akad. Nauk, Ser. Fiz*., **77** (1), 9 (2013).
26. Zabrodin I.G., Zakalov B.A., Kas'kov I.A., et al. *Poverkhnost'. Rentgenovskie, Sinkhrotronnye i Neitronnye Issledovaniya*, (9), 109 (2013).
27. Chkhalo N.I., Churin S.A., Pestov A.E., et al. *Opt. Express*, **22** (17), 20094 (2014).
28. Zorina M.V., Nefedov I.M., Pestov A.E., et al. *Poverkhnost'. Rentgenovskie, Sinkhrotronnye i Neitronnye Issledovaniya*, (8), 9 (2015).
29. Andreev S.S., Akhsakhalyan A.D., Bibishkin M.A., et al. *Cent. Eur. J. Phys*., **1**, 191 (2003).
30. Chkhalo N.I., Drozdov M.N., Kluenkov E.B., et al. *J. Micro/ Nanolith. MEMS MOEMS*, **11**, 021115 (2012).
31. Chkhalo N.I., Pestov A.E., Salashchenko N.N., et al. *Rev. Sci. Instrum*., **86**, 063701 (2015).